Chinese Journal of
POLYMER SCIENCE

RESEARCH ARTICLE

https://doi.org/10.1007/s10118-026-3663-0
Chinese J. Polym. Sci. **2026**, *44*, 2502–2512

Modulating Water Binding in Branched Poly(terphenylene 3-piperidinium) Anion Exchange Membranes for High-performance Water Electrolysis

Zhen-Jiang Yan[a,†], Bo Li[b,†], Chen-Xi Wang[a], Lan Zhang[a], Heng Wang[b], Hai-Bing Wei[a,c*], and Yun-Sheng Ding[a,c]

[a] *Department of Polymer Science and Engineering, School of Chemistry and Chemical Engineering, Hefei University of Technology, Hefei 230009, China*
[b] *State Key Laboratory of Organometallic Chemistry, Shanghai Institute of Organic Chemistry, University of Chinese Academy of Sciences, Chinese Academy of Sciences, Shanghai 200032, China*
[c] *Anhui Key Laboratory of Advanced Functional Materials and Devices, Hefei University of Technology, Hefei 230009, China*

Electronic Supplementary Information

Abstract Anion exchange membranes (AEMs) are central to clean energy technologies such as AEM water electrolysis, and clarifying how water binding and solvation govern ion transport and membrane swelling is critical to advancing their performance. Here, using a distorted, five-site branching agent, dispiro[fluorene-9,1′-3′-methylenecyclohexane-5′,9″-fluorene] (SFCF), we report branched poly(terphenylene 3-piperidinium) membranes that combine strong water binding with efficient ion transport. Upon polymer branching, the membranes exhibit a higher fraction of bound water and increased local molecular mobility while absorbing only half as much water as the linear analog. As a result, the optimized B-*i*PTP-3 delivers a high conductivity of 186 mS·cm^{-1} at 80 °C with a low 56 wt% water uptake and less than 15% swelling. In addition, by isomeric piperidinium chemistry, the membrane shows excellent alkaline stability in 1 mol·L^{-1} aq. NaOH, with no degradation after a 2000-h soaking at 80 °C. An AEM water electrolyzer equipped with the branched membrane achieves a high current density of up to10.4 A·cm^{-2} at 2 V. Moreover, the electrolyzer can operates stably at 1.0 A·cm^{-2} for 1000 h with a voltage decay of 95 μV·h^{-1}, without increased hydrogen crossover. This work highlights a branching-enabled design strategy for tuning water binding and solvation to realizing high performance, durable AEMs for clean energy devices.

Keywords Water electrolysis; Anion exchange membrane; Poly(terphenylene 3-piperidinium); Bound water; Alkaline stability

Citation: Yan, Z. J.; Li, B.; Wang, C. X.; Zhang, L.; Wang, H.; Wei, H. B.; Ding, Y. S. Modulating water binding in branched poly(terphenylene 3-piperidinium) anion exchange membranes for high-performance water electrolysis. *Chinese J. Polym. Sci*. **2026**, *44*, 2502–2512.

INTRODUCTION

Hydrogen is an energy carrier that, when produced from renewable sources, can deliver near-zero lifecycle emissions and is pivotal to energy transition and carbon neutrality goals.[1] However, most hydrogen is produced from fossil fuels, which have significant environmental impacts. Among the various production pathways, low-temperature water electrolysis is widely regarded as one of the most promising routes for clean hydrogen. Within this class, anion exchange membrane water electrolysis (AEMWE) has attracted growing attention over the past decade because it combines the low cost and benign alkaline environment of alkaline water electrolyzers (AWEs) with the high-performance and compact configuration of proton exchange membrane water electrolyzers (PEMWEs).[2]

Despite this promise, AEMWE systems remain at the laboratory or pilot scale. The instability of key components, including membrane degradation and mechanical failure,[3–5] metal dissolution from non-precious alloy electrodes,[6,7] and hydrogen crossover that raises the H_2-in-O_2 concentration during operation,[8,9] have thus far hindered its commercialization. As the core component of an AEMWE, the anion exchange membrane (AEM) serves three essential functions: transporting hydroxide ions (OH^-), suppressing gas crossover between the two electrodes, and physically separating the cathode and anode.[10] Consequently, the performance and durability of AEMWE depend critically on the ionic conductivity, chemical stability, and mechanical robustness of AEMs.

High-performance AEMs require a delicate balance between ion conductivity and water uptake.[11–13] Generally, owing to the low mobility of hydroxide relative to that of protons, an AEM with acceptable conductivity is often realized by an increased ion content, which is often described by a high ion exchange capacity (IEC). However, high IECs often leads to excessive water absorption and thereby over-swelling, which

* Corresponding author, E-mail: hbwei@hfut.edu.cn
† These authors contributed equally to this work.
Invited Research Article
Received March 8, 2026; Accepted March 11, 2026; Published online June 9, 2026

in turn reduces its mechanical integrity and chemical stability, resulting in a "conductivity-swelling" trade-off.[14] Similar to protons, hydroxide migrates through the membrane predominantly *via* a Grotthuss mechanism aided by transient hydrogen-bond rearrangements, and its mobility is highly related to the solvation of the incorporated cationic functionalities. Thus, to resolve this dilemma rationally, it is useful to consider the role of absorbed water in the membrane in governing OH^- transport and concomitant bulking swelling.

Water in AEMs can be broadly categorized as free (bulk-like) and bound water, which are either associated with cationic sites or confined within the intrinsic nanopores of the polymer skeleton.[15–17] Free water interacts weakly with the polymer and primarily drives macroscopic swelling, whereas bound water forms structured hydration shells and hydrogen-bond networks that facilitate efficient OH^- hopping. This distinction motivates a general design principle: increasing the fraction of bound water while suppressing excess free water to sustain percolated ion-conducting pathways without incurring a large volumetric swelling. For example, Shao *et al*. proposed a "water retention optimization" strategy by introducing hydrophilic Si—O bonds into the membrane matrix to increase the bound water content, yielding AEMs with improved ion conductivity and alkaline stability[18]; the enhanced solvation of hydroxide provides steric and electronic shielding of its negative charge, thereby reducing its nucleophilicity and suppressing attack on cationic sites.[19]

Beyond tuning the cation chemistry, the polymer architecture offers an effective lever for regulating water speciation.[20–22] Notably, polymer branching can efficiently trap water without compromising the ion-conducting moiety content, thereby improving the water balance within the membrane.[23,24] Leveraging this strategy, Lee and co-workers[25] introduced a triphenylbenzene branching unit into a poly(terphenylene piperidinium) backbone; relative to its linear analogue, the branched membrane exhibited a 36% reduction in swelling yet achieved slightly higher ionic conductivity (146.7 $mS \cdot cm^{-1}$ at 80 °C). Alternatively, a tetrabutched spirofluorene unit can be incorporated into a poly(biphenylene piperidinium) scaffold to form a branched microporous network.[26] Despite the incorporation of 30 mol% branching units, the resulting QPSPBPip-30% membrane still showed water uptake exceeding 85% at room temperature. Moreover, the interconnected microporous channels may increase gas permeability, which is undesirable for water electrolysis. Therefore, designing AEMs that couple balanced water uptake with efficient ion transport and low mechanical integrity compromise, as well as low gas permeability, is critical for high-performance AEMWE.

In this study, we designed and synthesized a novel five-site branching agent, dispiro[fluorene-9,1′-3′-methylenecyclohexane-5′,9″-fluorene] (SFCF), *via* a two-step method. Branched AEMs based on a poly(terphenylene 3-piperidinium) skeleton were synthesized *via* superacid-catalyzed polymerization for clean energy applications. The effects of the branching agent content (3 mol% and 5 mol%) on the water absorption behaviors, such as hydration states, bound water contents, ion conducting efficiency, and other membrane properties, were investigated, and the origin of conductivity enhancement in the branched membranes was elucidated. In addition, owing to the synergistic stability of the ether-free aromatic backbone and 3-piperidinium cations, the branched membrane exhibited no detectable degradation after exposure to 1 $mol \cdot L^{-1}$ NaOH at 80 °C for 2000 h. Finally, we assessed the AEMWE performance of B-*i*PTP-3, which delivered excellent water-electrolysis metrics, highlighting its potential for practical AEMWE applications.

EXPERIMENTAL

The experimental sections are described in the electronic supplementary information (ESI).

RESULTS AND DISCUSSION

Monomer Synthesis and Reactivity

Dispiro[fluorene-9,1′-3′-methylenecyclohexane-5′,9″-fluorene] (SFCF) was synthesized in two steps from commercially available fluorene following a modified procedure.[27] As illustrated in Fig. 1(a), difluorenylmethane was synthesized by reacting fluorene with polyoxymethylene in the presence of KOH in DMF. This intermediate was then treated with 3-chloro-2-(chloromethyl) propene in DMF using potassium *tert*-butoxide (KOtBu) as a base to yield SFCF in 50% yield. The structure of SFCF was confirmed by nuclear magnetic resonance (NMR) spectroscopy (Figs. S1 and S2 in ESI) and further validated by X-ray crystallographic analysis (Fig. 1b, CCDC 2512669). The X-ray diffraction data revealed that twisted methylenecyclohexane anchors two fluorenes in non-coplanar planes at an angle of 110.9°, resulting in a distorted, rigid, and non-rotatable conformation with dimensions of 8.06 Å × 6.52 Å × 5.26 Å. This unique configuration facilitates the formation of a dense, three-dimensional cross-linked network with five possible branching sites, which is expected to impart unique properties, such as enhanced water trapping and ion conduction, compared to linear polymers.[28]

Density functional theory (DFT) calculations were performed to investigate the reactivity of SFCF in the superacid-catalyzed hydroxyalkylation. The simulated structure of SFCF closely matched the structural parameters obtained from the X-ray crystallographic analysis, indicating the high accuracy of the theoretical calculations. As shown in Fig. 1(c), the electrostatic potential of the fluorene ring in SFCF was −0.021 eV, suggesting high electrophilicity. Similar values were observed for other well-studied fluorene-based spiros, such as spiro[cyclohexane-1,9′-fluorene] (CHF)[17] and spirobifluorene (SF),[29] which exhibited electrostatic potentials of −0.023 and −0.020 eV, respectively. This confirmed the high electrophilicity of the fluorene units in SFCF, enabling smooth hydroxyalkylation reactions with piperidone derivatives.

To further elucidate the reactive sites of SFCF, electrophilic indices of the potential reaction sites were calculated using the Fukui function (Fig. 1d). The *para*-position of the fluorene ring exhibited a high electrophilic index (0.045), whereas the *meta*-position showed a lower value (0.030), indicating that the para-position is the most probable active site for electrophilic reactions. This finding aligns with the high reactivity observed for fluorene-based arenes in the superacid-catalyzed hydroxyalkylation.[30,31] Additionally, the reactivity of

the terminal vinyl group on cyclohexane, which may also participate in electrophilic reactions, was investigated. A model reaction was carried out, and the resulting cross-linked products were analyzed by ^{13}C solid-state NMR (ssNMR) spectroscopy (Scheme S1 and Fig. S3 in ESI). When the monomer piperidin-3-one hydrochloride was reacted with SFCF in excess of 20%, that is, the molar ratio of SFCF and peridin-3-one hydrochloride was 1:3 molar ratio, the ^{13}C ssNMR signals of the terminal vinyl groups disappeared in the obtained cross-linked network, suggesting that this group is indeed a reactive site, making SFCF a pentafunctional monomer.

Polymer Synthesis

Given the high reactivity and pentafunctional nature of SFCF, incorporating a high ratio of SFCF induces significant cross-linking of the reaction system, complicating the subsequent solution-processed membrane fabrication. Therefore, a controlled amount of SFCF was introduced into a reaction system containing terphenyl and peridin-3-one hydrochloride in the presence of trifluoromethanesulfonic acid (TFSA) to afford branched ionomer B-*i*PTP-*x*, where *x* is the molar ratio (in percent) of SFCF to the terphenyl monomer (Scheme 1).

As previously demonstrated, finite-sized SFCF possesses five branching sites, which significantly enhance the local cross-linking degree in the polymer structure. Compared to the synthesis of linear *i*PTP, the introduction of SFCF markedly increased the viscosity of the reaction system. Specifically, the resultant B-*i*PTP-3 demonstrated an inherent viscosity (η_{inh}) of 3.60 dL·g^{-1}, indicative of a high-molecular-weight polymer upon branching (Table 1). When the molar ratio of SFCF was further increased to 5 mol%, despite the viscosity of the reaction system was improved accordingly, the resultant neutral piperidine-based precursor could not fully dissolve, suggesting a slight cross-linking occurred. Therefore, the insoluble polymer fractions were removed and the filtered solu-

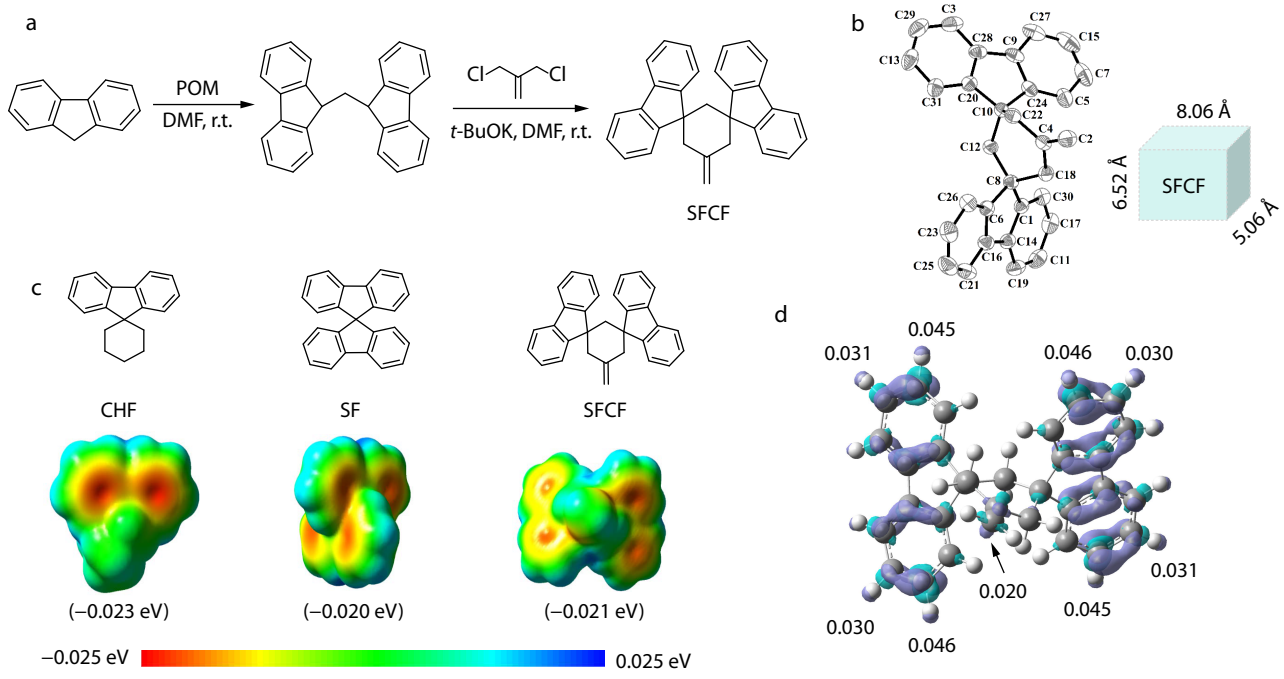

Fig. 1 Synthesis and structure for monomer SFCF. (a) Synthetic procedures and (b) single-crystal structure of SFCF. The molecular structure of SFCF was determined by single-crystal X-ray diffraction. Atoms are drawn at the 50% probability level. (c) Electrostatic potentials of SFCF determined by density functional theory (DFT) calculations. Two other spiros based on fluorene, CHF and SF, were also investigated for comparison. (d) The electrophilicity of partial carbon atoms in SFCF calculated by using Fukui functions.

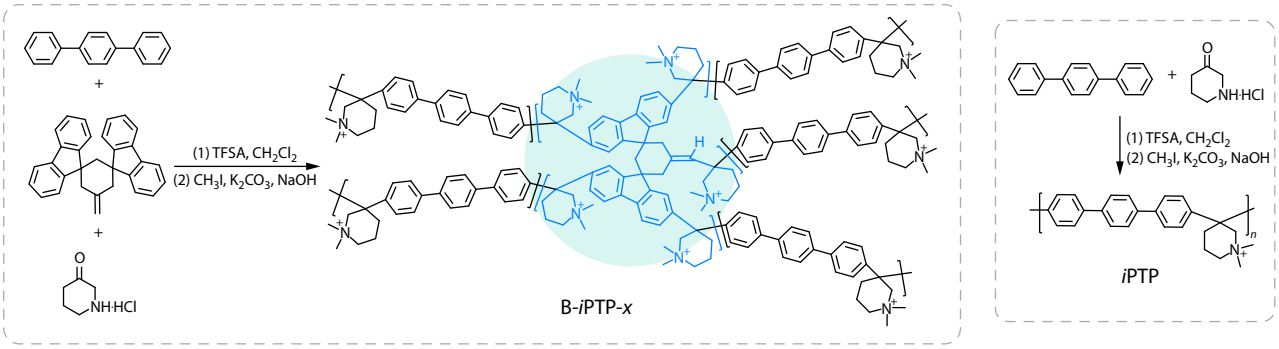

Scheme 1 Synthetic routes for the branched ionomers B-*i*PTP-*x* and the linear counterpart *i*PTP.

https://doi.org/10.1007/s10118-026-3663-0

Table 1 Properties of the branched and linear poly(terphenylene 3-piperidinium) membranes.

Sample	IEC_w (mmol·g^{-1})	Viscosity [a] (dL·g^{-1})	WU [b] (wt%)		SR [b] (%)		$\sigma(OH^-)$ [c] (mS·cm^{-1})		λ [d]
			30 °C	80 °C	30 °C	80 °C	30 °C	80 °C	
*i*PTP	2.78	1.14	83.0	107.8	20.7	30.2	87.8	180.2	16.57
B-*i*PTP-3	2.81	3.60	47.3	56.1	10.0	14.9	97.4	185.6	9.34
B-*i*PTP-5	2.87	3.42	52.5	67.9	12.8	16.3	102.7	189.0	10.15

[a] Determined by using an Ubbelohde viscometer at (25±0.1) °C in DMSO at a concentration of 0.5 g·dL^{-1}; [b] Measured in deionized water with OH^- form membrane (immersed, average of two measurements); [c] Measured in the OH^- form by an *in situ* OH^- exchanging method; [d] Hydration number, calculated from the number of absorbed water molecules per piperidinium moieties.

ble parts were subjected to subsequent methylation to afford ionomeric B-*i*PTP-5. As a result, a slight decrease in the viscosity of B-*i*PTP-5 (3.42 dL·g^{-1}) was observed, consistent with observations reported by Lee *et al*.[23]

In addition to the observed increase in viscosity, the incorporation of SFCF units was further confirmed by ^{1}H-NMR spectroscopy (Fig. S4 in ESI). In comparison to the linear *i*PTP, two additional small peaks with the chemical shifts of 7.35 and 7.45 ppm, assigning to the protons from fluorene units, were detected in the branched B-*i*PTP-*x*. This confirms the successful integration of the SFCF. Additionally, peak broadening was observed in the branched samples, indicating decreased solubility in deuterated solvents or slight variations in the chemical environment, reflecting the presence of branching units.

Water Absorption Behaviors and Ion Conductivity

Water content is a key parameter that affects nearly all physicochemical properties of the AEM and, consequently, its electrochemical performance.[12] Ideally, an AEM with a high IEC and relatively low water uptake (*i.e.*, a low hydration number) can achieve high ionic conductivity, as it follows the relation $\sigma = F[X^-]\mu_{X^-}$, where F is Faraday's constant, and $[X^-]$ and μ_{X^-} denote the anion concentration and mobility, respectively. The water uptake of linear *i*PTP showed a value of 107.8 wt% at 80 °C, while the branched analogues B-*i*PTP-3 and B-*i*PTP-5 exhibited lower values of 56.2 wt% and 67.9 wt%, respectively (Fig. 2a). This pronounced suppression of water uptake in the branched samples likely arises from branching-induced intrachain interactions that restrict swelling of the hydrophilic domains.[32] It is worth noting that because insoluble cross-linked fractions were removed during polymer synthesis, B-*i*PTP-5 absorbed slightly more water than B-*i*PTP-3, which is in accordance with the lower viscosity of B-*i*PTP-3. Consistent with the water uptake trends, the in-plane swelling ratios of the branched membranes were lower than those of the linear control. Specifically, compared to *i*PTP (20.7% at room temperature), B-*i*PTP-3 showed a marked

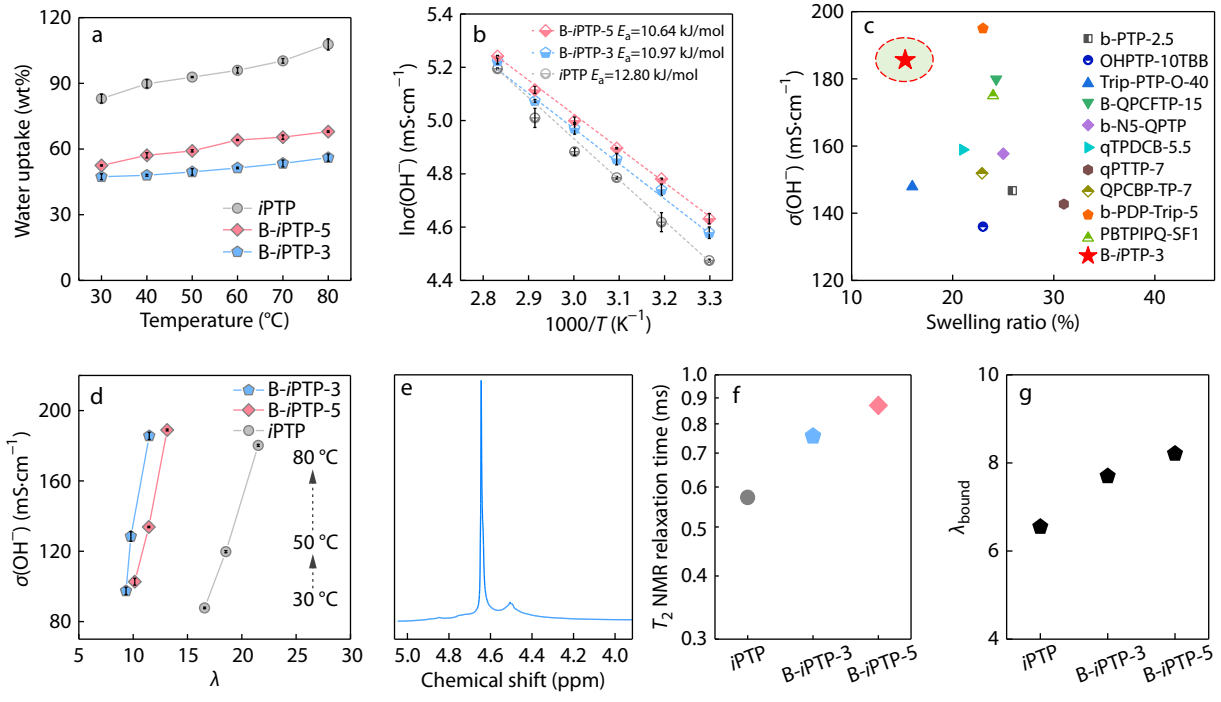

Fig. 2 Water absorption behaviors and ion conductivity. (a) Water uptake of B-*i*PTP-*x* and *i*PTP membranes in OH^- form at fully hydrated states (immersed) as a function of temperature; (b) Hydroxide conductivities as a function of temperature and the calculated activation energies (E_a) for ion transportation; (c) The comparative image of conductivity and swelling ratio of B-*i*PTP-3 membrane at 80 °C against other reported AEMs. References for data points: b-PTP-2.5,[25] OHPTP-10TBB,[33] Trip-PTP-O-40,[34] B-QPCFTP-15,[35] b-N5-QPTP,[36] qTPDCB-5.5,[37] QPCBP-TP-7,[38] qPTTP-7,[39] PBTPIPQ-SF1,[29] b-PDP-Trip-5.[23] (d) Hydroxide conductivities of B-*i*PTP-*x* membranes as a function of hydration number λ; (e) ^{1}H-NMR spectrum of B-*i*PTP-3 membrane (OH^- form) in D_2O; (f) T_2 calculated from the full-width at half-maximum of water peaks; (g) Bound water molecules (λ_{bound}) of B-*i*PTP-*x* and *i*PTP membranes in OH^- form as a function of degrees of branching.

decrease of 10.0% (Table 1 and Fig. S5 in ESI). As noted above, membranes that combine a high ion content with minimal swelling are desirable, as they facilitate device assembly and ensure efficient interfacial contact with both electrodes.

Hydroxide conductivity measured between 30–80 °C reveals that the branched membranes (B-*i*PTP-*x*) maintain slightly higher conductivity than the linear analog, despite absorbing only half as much water as *i*PTP (Fig. 2b). At 80 °C, B-*i*PTP-3 and B-*i*PTP-5 achieve 185.6 and 189.0 mS·cm^{-1}, respectively, placing them among the most conductive AEMs reported under comparable conditions (Fig. 2c and Table S2 in ESI). These results indicate more efficient use of water for ion transport in the branched architecture (Fig. 2d). Arrhenius analysis (lnσ~1/T) yields activation energies (E_as) that are 1.8–2.2 kJ·mol^{-1} lower for the branched membranes than for the linear *i*PTP (E_a=12.80 kJ·mol^{-1}), consistent with facilitated hydroxide transport pathways in the branched network.

To investigate the origin of this efficiency, we examined the state of water within the branched membranes. Water in AEMs can be categorized into free (bulk-like) and bound (associated with cationic sites) states.[18,40] Free waters predominantly govern macroscopic swelling, whereas efficient OH^- transport depends on sufficient bound water to sustain percolated, hydrated ion domains. As evidenced by ^{1}H-NMR, in a fully hydrated state, the branched membrane exhibits two water proton signals at 4.64 and 4.50 ppm, assigned to free and bound water, respectively (Fig. 2e), confirming the coexistence of distinct hydration environments.[16,26,28] Low-field NMR further differentiates the two states: free water exhibits long transverse relaxation times (T_2 >100 ms), whereas bound water shows much shorter T_2 values (<1 ms) (Fig. S6 in ESI). The measured bound-water T_2 increased from 0.572 ms in the linear *i*PTP to 0.756 ms in B-*i*PTP-3 and 0.870 ms in B-*i*PTP-5 (Fig. 2f), indicating that although the water remained in the bound regime, its local mobility was slightly higher in the branched membranes.[16] This trend is consistent with the relatively concentrated cationic domains in the branched architecture that lower the transport barriers for hydroxide ions and enable high conductivity at comparatively low overall water uptake.

To further quantify the water states in the AEM, differential scanning calorimetry (DSC) was used to measure the melting enthalpy of the water confined within the membrane matrix (Fig. S7 in ESI).[15,40] For *i*PTP with high water uptake, a prominent endothermic peak appears near 0 °C, attributable to the melting of free water. In contrast, B-*i*PTP-3 and B-*i*PTP-5 with lower water content exhibited no well-defined melting peaks, indicating that a large fraction of water was bound (non-freezing). The free water content was determined by comparing the melting enthalpy of the water in the membrane with that of pure water (Eq. S6 in ESI) to obtain the bound water content. As depicted in Fig. 2(g), the bound-water hydration number (λ_{bound}) is 6.55 for *i*PTP, increasing to 7.70 for B-*i*PTP-3 and further to 8.21 for B-*i*PTP-5 with incorporation of (SFSC branching unit. Thus, these branching networks promote the clustering of cationic groups within confined domains, enrich bound water, and form favorable percolated pathways, thereby enhancing the hydroxide conductivity while suppressing excessive swelling.

Mechanical Properties and Thermal Stability

AEMs used in alkaline water electrolysis devices are subjected to mechanical compressive stresses and repeated flushing with a liquid-supporting electrolyte, requiring them to exhibit excellent mechanical robustness, including high tensile strength and toughness. Furthermore, a significant trend in the development of advanced AEMWE is the fabrication of highly robust AEMs that can operate under pressure conditions (up to 3 MPa or even higher) without membrane failure or induced high gas crossover.[41] To our delight, all the prepared AEMs demonstrated high mechanical robustness, with tensile strengths exceeding 50 MPa (Fig. 3a). The branched sample B-*i*PTP-3 exhibited higher tensile strength and toughness than its linear counterpart, *i*PTP. B-*i*PTP-3 exhibited a tensile strength of 57 MPa and toughness of 17.1 MJ·m^{-3}. The enhanced mechanical robustness of B-*i*PTP-3 can be attributed to improved intermolecular interactions facilitated by polymer branching and suppressed water absorption. Reduced water absorption minimizes the presence of free water, which would otherwise weaken inter-

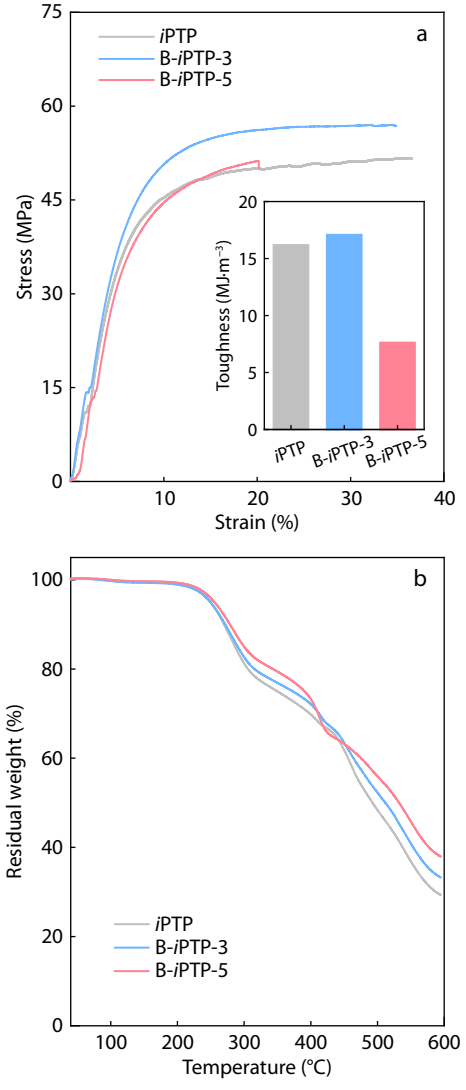

Fig. 3 (a) The stress-strain curves and toughness of the B-*i*PTP-*x* membranes in I^- form under the atmosphere; (b) TGA curves of the B-*i*PTP-*x* membranes in I^- form. (in N_2 atmosphere at the heating rate of 10 °C·min^{-1}).

https://doi.org/10.1007/s10118-026-3663-0

chain interactions and degrade the mechanical integrity of the membrane. However, it should be noted that, for the B-*i*PTP-5 membrane, a higher feed ratio of the SFCF monomer makes the polymer difficult to dissolve. As a result, B-*i*PTP-5 fabricated from the filtered solution may exhibit a lower molecular weight or branching degree, resulting in decreased tensile strength (51.2 MPa) and elongation at break (20%).

The thermal stability of the AEMs was assessed by thermogravimetric analysis (TGA) under a nitrogen atmosphere. As depicted in Fig. 3(b), the incorporation of SFCF branching units did not alter the thermal stability of the AEMs, which exhibited a degradation behavior similar to that of its linear counterpart. Within the temperature range of 220–300 °C, the observed mass loss corresponds to the degradation of piperidinium functionalities. Above 310 °C, extensive thermal decomposition of the polymer backbone occurs. Therefore, under the application of water electrolysis and other electrochemical devices, the branched B-*i*PTP membranes exhibited satisfactory thermal stability.

The above data suggest that B-*i*PTP-3 is the most promising, owing to its favorable OH^- conductivity, resistance to water absorption and swelling, excellent mechanical properties, and high thermal stability. Consequently, B-*i*PTP-3 was selected for further tests of alkaline stability, water electrolysis device performance, and device durability, highlighting its potential for advanced AEMWE applications.

Chemical Stability

Alkaline stability is a particularly important parameter for the AEM used in alkaline electrochemical devices. Despite significant progress in enhancing the alkaline stability of piperidinium functionalities, poly(arylene piperidinium) (PAP) membranes still undergo degradation *via* *β*-H Hoffmann elimination, which affects the durability of AEMs during long-term operation in electrolyzers.[4,42,43] Recently, our group demonstrated that a structural modification, specifically, repositioning the *N*,*N*-dimethylpiperidinium (DMP) group from the *γ*-position to the *β*-position on PAP backbones, altered the dihedral angle of the *β*-H—C—C—N moiety, thereby increasing the Hofmann elimination energy barrier.[44] This modification significantly suppressed Hofmann degradation under high pH conditions, resulting in improved long-term alkaline durability of the AEMs (Fig. 4A). As expected, this isomerization strategy positively affected the stability of the resulting AEMs. To evaluate alkaline stability, the B-*i*PTP-3 membrane was soaked in 1 mol·L^{-1} and 5 mol·L^{-1} NaOH aqueous solutions for 2000 and 1080 h, respectively, and the loss of piperidinium moieties was determined by ^{1}H-NMR analysis. As shown in Fig. 4(B), after soaking in 1 mol·L^{-1}

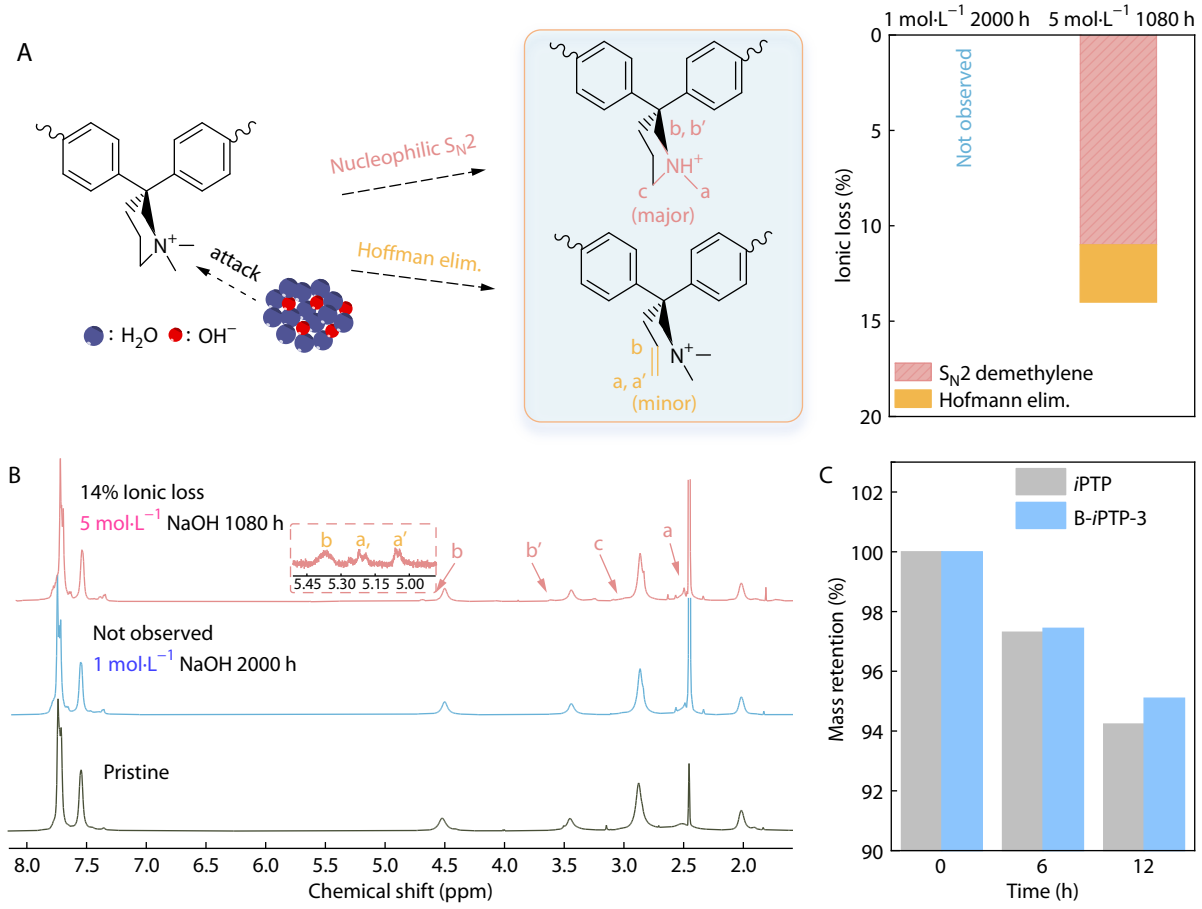

Fig. 4 (A) Proposed degradation products *via* Hofmann elimination and de-methylation pathways, and loss of piperidinium groups in the membranes after the alkaline treatment; (B) ^{1}H-NMR spectra of B-*i*PTP-3 membrane before and after alkaline treatment during 2000 h in 1 mol·L^{-1} NaOH and 1080 h in 5 mol·L^{-1} NaOH at 80 °C, respectively; (C) Remaining mass of the *i*PTP and B-*i*PTP-3 membranes after the hot Fenton's degradation (3 mg·L^{-1} $FeSO_4$ and 3 wt% H_2O_2, 60 °C).

https://doi.org/10.1007/s10118-026-3663-0

aq. NaOH for 2000 h, all the characteristic protons in the B-*i*PTP-3 membrane were well retained, and no decay in the integrals was observed. These results indicate that the piperidinium moieties in B-*i*PTP-3 exhibit high durability in 1 mol·L^{-1} NaOH, which is the most commonly used alkali concentration in AEMWEs.

Furthermore, an accelerated degradation test was performed in 5 mol·L^{-1} aq. NaOH for 1080 h. After treatment, the membrane remained ductile with its surface intact, and no defects were detected (Fig. S8 in ESI). However, under these stringent conditions, the B-*i*PTP-3 membrane experienced a 14% loss in the piperidinium groups (Fig. 4B). From the integrals of the new protons emerged at 5.1, 5.3, and 5.4 ppm, it was determined that only 3% of the total piperidinium group loss in B-*i*PTP-3 was due to Hofmann elimination, indicating that this degradation pathway, typically dominant in conventional poly(arylene piperidinium)s,[43,45] was substantively suppressed. In contrast, demethylation *via* the S_N2 nucleophilic substitution pathway became the dominant degradation route. Nonetheless, the isomerization strategy enabled branched AEM B-*i*PTP-3 to demonstrate excellent alkaline stability by effectively suppressing the Hofmann elimination degradation pathway.

In addition to the alkaline stability, the oxidative stability of the membrane should not be overlooked, as the polymer backbone also undergoes scission due to oxidative degradation.[46] To evaluate the oxidative stability of the AEMs, we performed accelerated degradation experiments using Fenton's reagent (3 mg·L^{-1} Fe^{2+}, 3 wt% H_2O_2). As shown in Fig. 4(C), after 6-h of immersion in Fenton's reagent, the mass retention of both linear *i*PTP and branched B-*i*PTP-3 membranes exceeded 97%, indicating a certain degree of antioxidant properties. However, after 12 h of prolonged immersion, the mass retention of B-*i*PTP-3 was 95.1%, which is slightly higher than that of the linear *i*PTP membrane (94.2% retention). We hypothesized that the slightly improved oxidative stability of B-*i*PTP-3 may be attributed to the incorporation of hyperbranched SFCF units, which alleviates the packing interactions between the electron-rich backbones. This reduction in packing behavior slows down the reaction of $O^{\bullet-}$ abstracting hydrogen atoms, thereby enhancing the oxidation stability of the B-*i*PTP-3 membrane.[47] Additionally, the reduced water absorption in B-*i*PTP-3 mitigated the direct interaction between the internal water and the polymer framework, further decreasing the attack of free radicals and moderating the degradation of the main chain.[38]

Water Electrolysis Performance

To further assess the practical applications of the branched membranes in water electrolysis, B-*i*PTP-3 was assembled into a water electrolyzer. The catalysts used were Ni-Fe LDH (CAPist L1)[48] and Pt/C (0.5 mg·cm^{-2}) for the anode and cathode, respectively, with the catalysts incorporated using the catalyst-coated substrate (CCS) and catalyst-coated membrane (CCM) assembly methods (Fig. S9 in ESI). As illustrated in Fig. 5(a), the B-*i*PTP-3-based device demonstrated a higher water electrolysis performance than its linear *i*PTP counterpart. At 60 and 80 °C, the current densities of the B-*i*PTP-3 membrane reached 4.18 and 6.28 A·cm^{-2}, respectively, outperforming the linear *i*PTP sample, which exhibited current densities of 4.06 A·cm^{-2} at 60 °C and 5.70 A·cm^{-2} at 80 °C. Given the same assembly and operating conditions, this difference in performance is likely related to the higher conductivity of B-*i*PTP-3. Additionally, electrochemical impedance spectroscopy (EIS) analysis supported these observations, showing that the ohmic resistance (R_{ohm}) of the B-*i*PTP-3-based electrolyzer was 0.098 Ω·cm^{-2} at 80 °C, whereas the *i*PTP-based device had a R_{ohm} of 0.103 Ω·cm^{-2} (Fig. S10 in ESI). These results highlight the advantages of the B-*i*PTP-3 membrane for AEMWE applications.

Subsequently, the effect of temperature (ranging from 40 °C to 80 °C) on the electrolyzer performance was assessed. As the operating temperature decreased from 80 °C to 40 °C, the current density of the electrolyzer based on B-*i*PTP-3 dropped from 6.28 A·cm^{-2} to 2.39 A·cm^{-2} at 2.0 V, as indicated by the increased R_{ohm} and charge transfer resistance (R_{ct}) (Fig. 5b and Fig. S11 in ESI). Notably, even at 60 °C, the B-*i*PTP-3-based AEMWE still delivered a current density of 2.31 A·cm^{-2} at 1.8 V, exceeding the U.S. Department of Energy's 2026 target for AEM electrolyzers (2.0 A·cm^{-2} at 1.8 V). This high performance suggests that the membrane is suitable for use in industrial-scale electrolyzers, as its low operating voltage (under a constant current density, for example, 1.0 A·cm^{-2}) can significantly mitigate ionomer oxidation scission and improve power efficiency. Furthermore, the catalyst activity directly influences the electrolyzer performance. When the Ni-Fe catalyst in the anode was replaced with Ir, an impressive performance with a current density of 10.4 A·cm^{-2} at 2.0 V and 80 °C was achieved (Fig. 5c). Even at 40 °C, the fabricated AEMWE still exhibited a current density of 4.30 A·cm^{-2} at 2.0 V, demonstrating an excellent water electrolysis performance.

The gas barrier property of the membrane is a crucial parameter for the AEMWE. Membranes with excellent gas-barrier properties effectively inhibit gas crossover, thereby enhancing the benefits of the zero-gap configuration and ensuring safe operation.[9] One of the key parameters for evaluating the gas barrier performance of membranes in AEM water electrolysis is the hydrogen-to-oxygen (HTO) ratio. Using the targets set by the U.S. DOE for electrolyzers as a benchmark (the technical safety limit for the emergency shutdown of the electrolyzer system is 2.0 vol%), we evaluated the HTO of the B-*i*PTP-3 membrane under different current densities. As shown in Fig. 5(d), the HTO content of B-*i*PTP-3-based electrolyzer is as low as 0.10 vol% at 60 °C and 1.0 A·cm^{-2}. Even at an extremely low current density (0.1 A·cm^{-2}, the HTO value increases only to 0.55 vol%, which remains well below the 2.0 vol% safety limit (specific values are provided in Table S3 in ESI). The suppressed water absorption of B-*i*PTP-3 may be responsible for the observed good gas barrier properties, enabling it to be compatible with the AEMWE system. Furthermore, the low gas permeability of the membrane enhanced the Faradaic efficiency of the water electrolysis device. To evaluate this, the hydrogen produced at the cathode was measured and compared with theoretical values. Over a 30-minute monitoring period, the flow rate of the generated hydrogen remained steady and closely matched the theoretical value, achieving a Faradaic efficiency of over 99% (Fig. 5e). Thus, the combination of low HTO and high Faradaic efficiency confirmed that the B-*i*PTP-3 membrane exhibited excellent gas tightness and high current conversion efficiency during continuous water electrolysis.

https://doi.org/10.1007/s10118-026-3663-0

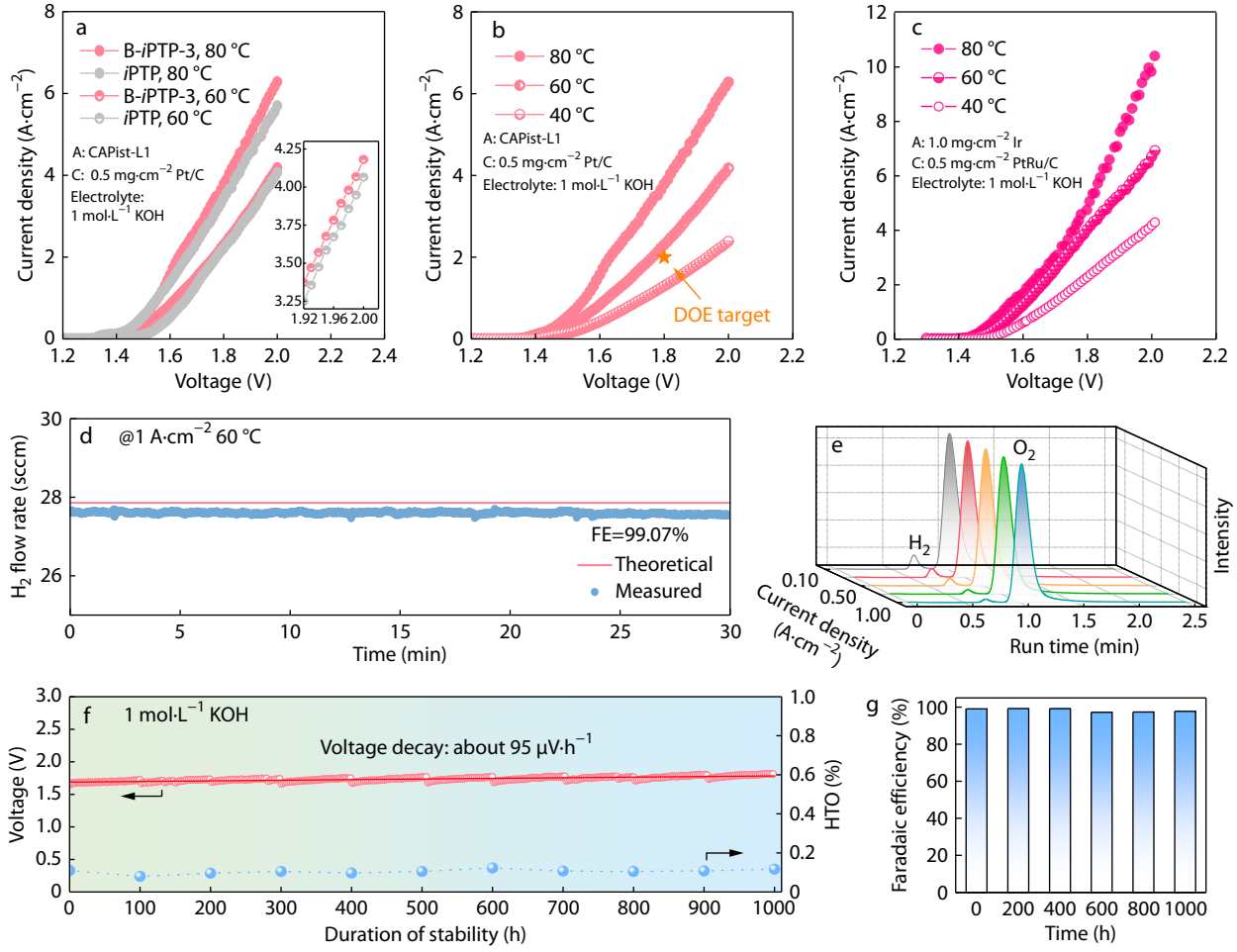

Fig. 5 Water electrolysis performance. (a) IV curves of the *i*PTP and B-*i*PTP-3-based AEMWEs using a non-precious-metal anode catalyst, Ni-Fe LDH, and a Pt/C cathode at 60 and 80 °C. The membrane thickness for all water electrolyzer assemblies is (40±2) μm. (b) Temperature-dependent polarization curves of the B-*i*PTP-3-based AEMWE; (c) The polarization curves of the AEMWE based on Ir anode (1.0 mg·cm^{-2} Ir) and Pt-Ru/C cathode (0.5 mg·cm^{-2} Pt-Ru, 60% Pt-Ru on Carbon black, Pt/Ru = 1/1) at different temperatures. An asymmetric pressure of 100 kPa was applied to the anode. (d) Theoretical and measured H_2 flow rates for the B-*i*PTP-3-based electrolyzer under 1.0 A·cm^{-2} at 60 °C; (e) Gas chromatography (GC) spectra of the gas escaping from the anode of the B-*i*PTP-3-based cell under different current densities at 60 °C; (f) Durability of the water electrolyzer fabricated of B-*i*PTP-3 under 1.0 A·cm^{-2} for 1000 h, along with the HTO values during this period. The fresh 1 mol·L^{-1} KOH solution was replaced every 100 h. (g) Faradaic efficiency of the MEAs under 1 A·cm^{-2} during a 1000-h durability test.

Thereafter, a 1000-h long-term water electrolysis test was conducted at 60 °C and 1.0 A·cm^{-2}. During this time, the applied voltage, HTO, and Faradaic efficiency were monitored continuously. As depicted in Fig. 5(f), the water electrolysis system operated stably as the applied voltage increased from 1.649 V to 1.813 V. Specifically, during the first 300 h, the voltage increased slightly; however, after replacing the KOH solution with fresh electrolyte, the voltage returned to approximately 1.65 V. This phenomenon may be attributed to the generation of bubbles during continuous electrolysis, which increases mass transfer resistance (R_{mt}).[49] Hence, replacing the electrolyte and flushing the flow channels was conducive to bubble escape, allowing the cell to restore its initial performance. However, after that, an irreversible voltage loss gradually occurred, leading to a decline in the long-term operation. This voltage decay is likely associated with the interface failure between the membrane and catalyst layer, particularly at the cathode, as evidenced by the exfoliation of the catalyst layer from the membrane after 1000-h of operation (Fig. S12 in ESI). To confirm possible cationic group degradation or changes in the polymer structure, NMR analysis of the aged membrane was performed. As shown in Fig. S13 (in ESI), no new proton signals emerged for the aged B-*i*PTP-3 membrane, indicating that the membrane maintained good tolerance, which is consistent with the *ex situ* alkaline stability of the membrane in 1 mol·L^{-1} NaOH for 2000 h at 80 °C.

On the other hand, despite no detectable degradation in B-*i*PTP-3 membrane, the polarization curves of B-*i*PTP-3-based MEA show a performance degradation of 13% under 60 °C (from initial 4.18 A·cm^{-2} to 3.63 A·cm^{-2} at 2.0 V) (Fig. S14 in ESI). The EIS plots before and after the long-term stability test also corroborated this conclusion, where the increase in HFR was likely attributed to the compromised interfacial contact between the catalytic layer and the membrane after long-term operation, whereas the increase in R_{ct} may be attributed to the agglomeration and aging of catalysts within the catalytic layer (Fig. S15 in ESI). Nevertheless, throughout the en-

tire 1000-h durability test, the B-*i*PTP-3-based electrolysis device exhibited a voltage decay of 95 μV·h^{-1}, making it one of the most durable AEMWE devices. Moreover, during 1000 h of operation, the HTO of the device remained consistently around 0.1 vol%, and the Faradaic efficiency was maintained at about 98% (Figs. 5f and 5g), suggesting the excellent long-term integrity of the B-*i*PTP-3 membrane. The high alkaline stability of the B-*i*PTP-3 membrane enabled the electrolyzer to operate with fully PGM-free electrodes (Anode: CAPist-L1; Cathode: Ni-Mo) in 5 mol·L^{-1} KOH electrolyte, achieving a current density of 3.76 A·cm^{-2} at 2.0 V (Fig. S16 in ESI). Moreover, during 300 h of operation at 60 °C under a current density of 0.50 A·cm^{-2}, a negligible voltage rise of 15 μV·h^{-1} was observed. These findings further emphasize the potential of the B-*i*PTP-3 membrane for practical water electrolysis applications.

CONCLUSIONS

In summary, by incorporating a distorted five-site branching agent, we designed and synthesized branched poly(terphenylene 3-piperidinium) membranes that increase the fraction of bound water and promote efficient ion transport. Branching enables high hydroxide conductivity while substantively suppressing the water uptake and dimensional swelling. The optimized membrane, B-*i*PTP-3, achieves simultaneously high conductivity of 186 mS·cm^{-1} along with reduced water uptake and swelling (<15%) at 80 °C. In AEM water electrolysis, cells assembled with the branched membrane reach 10.4 A·cm^{-2} with an Ir anode and 6.3 A·cm^{-2} with a Ni-Fe PGM-free anode, and operate stably for over 1000 h. The strategy of tuning water binding using distorted multi-site branching was established to develop high-performance, durable AEMs for clean energy generation.

Conflict of Interests

The authors declare no interest conflict.

Electronic Supplementary Information

Electronic supplementary information (ESI) is available free of charge in the online version of this article at http://doi.org/10.1007/s10118-026-3663-0.

Data Availability Statement

The data supporting the findings of this study are available from the corresponding author reasonable request.

ACKNOWLEDGMENTS

We thank Mr. Weizhe Zhang at Tsinghua University for collecting the data of AEMWE measurements based on the Ir anode. This work was financially supported by the National Natural Science Foundation of China (Nos. 52273205 and 22271198) and Fundamental Research Funds for the Central Universities (No. JZ2024HGTG0297).

REFERENCES

1 McKenna, R.; Staffell, I. Realistic roles for hydrogen in the future energy transition. *Nat. Rev. Clean Technol.* **2025**, *1*, 351–371.
2 Du, N. Y.; Roy, C.; Peach, R.; Turnbull, M.; Thiele, S.; Bock, C. Anion-exchange membrane water electrolyzers. *Chem. Rev.* **2022**, *122*, 11803–11895.
3 Maxwell, D. S.; Kendrick, I.; Mukerjee, S. Operando raman spectroscopy reveals degradation byproducts from ionomer oxidation in anion exchange membrane water electrolyzers. *J. Am. Chem. Soc.* **2024**, *146*, 22431–22444.
4 Yin, L. Q.; Ren, R.; He, L. L.; Lee, H.; Zhang, Q. H.; Ding, G. H.; Wang, L. Q.; Sun, L. C. Polyarylmethylpiperidinium (PAMP) for next generation anion exchange membranes. *Angew. Chem. Int. Ed.* **2025**, *64*, e202503715.
5 Wang, T.; Ma, M. X.; Chen, W. J.; Zuo, Y. F.; Wei, H. B.; Ding, Y. S. Reinforced poly(arylene quinuclidinium) membranes for anion exchange membrane water electrolysis. *Chinese J. Polym. Sci.* **2025**, *43*, 2386–2394.
6 Li, W. L.; Ding, Y. X.; Zhao, Y. L.; Li, Z. H.; Lin, G. X.; Wang, L. Q.; Sun, L. C. Zwitterion-modified NiFe OER catalyst achieving ultrastable anion exchange membrane water electrolysis *via* dynamic alkaline microenvironment engineering. *Angew. Chem. Int. Ed.* **2025**, *64*, e202505924.
7 Rajeev, M.; Jerome-Saboori, A.; Shekhar, R.; Boettcher, S. W.; Kempler, P. A. Impacts of dissolved iron on alkaline water electrolysis cells. *ACS Catal.* **2025**, *15*, 2847–2856.
8 Tan, A. D.; Song, J. Y.; Qiu, X. T.; Liu, Z.; Xia, L. F.; Ju, C.; Zhao, F.; Li, G.; Shi, X. Y.; Li, T. T.; Liu, P.; Liu, J. Catastrophic localized deflagration formation mechanisms and safety precautions in proton exchange membrane water electrolyzer. *Nat. Commun.* **2025**, *16*, 9115.
9 Hu, C.; Lee, J. Y.; Lee, Y. J.; Kim, S. H.; Hwang, H.; Yoon, K.-s.; Park, C.-d.; Lee, S. Y.; Lee, Y. M. Reinforced poly(dibenzyl-co-terphenyl piperidinium) membranes for highly durable anion-exchange membrane water electrolysis at 2 A·cm^{-2} for 1000 h. *Next Energy* **2023**, *1*, 100044.
10 Henkensmeier, D.; Cho, W. C.; Jannasch, P.; Stojadinovic, J.; Li, Q. F.; Aili, D.; Jensen, J. O. Separators and membranes for advanced alkaline water electrolysis. *Chem. Rev.* **2024**, *124*, 6393–6443.
11 Kim, Y.; Wang, Y.; France-Lanord, A.; Wang, Y.; Wu, Y.-C. M.; Lin, S.; Li, Y.; Grossman, J. C.; Swager, T. M. Ionic highways from covalent assembly in highly conducting and stable anion exchange membrane fuel cells. *J. Am. Chem. Soc.* **2019**, *141*, 18152–18159.
12 Overton, P.; Li, W.; Cao, X.; Holdcroft, S. Tuning ion exchange capacity in hydroxide-stable poly(arylimidazolium) ionenes: increasing the ionic content decreases the dependence of conductivity and hydration on temperature and humidity. *Macromolecules* **2020**, *53*, 10548–10560.
13 Yadav, V.; Miyatake, K.; Mahmoud, A. M. A.; Xian, F.; Liu, F.; Guo, L. Poly(fluorene)-based anion exchange membranes, part 1: effect of pendant alkyl chain length on membrane properties. *Macromolecules* **2025**, *58*, 10787–10799.
14 Olsson, J. S.; Pham, T. H.; Jannasch, P. Tuning poly(arylene piperidinium) anion-exchange membranes by copolymerization, partial quaternization and crosslinking. *J. Membr. Sci.* **2019**, *578*, 183–195.
15 Liu, X. D.; Chen, X. H.; Pei, S. P.; Li, H.; Zhang, Y. M. Evaluation of water in perfluorinated anion exchange membranes with different IEC values. *J. Phys. Chem. C* **2017**, *121*, 17546–17551.
16 Pang, M.; Xu, Z.; Lin, D.; Zhen, Y.; Tian, J.; Liu, J.; Xu, Q.; Wang, B. Facilitating rapid OH^-/H_2O transport in anion exchange membranes *via* ultra-stable heteroatom-free micropores. *Angew. Chem. Int. Ed.* **2024**, *64*, e202418435.
17 Wang, T.; Zhang, W.; Wang, T.; Jiang, T.; Zhu, C.; Liu, C.; Shi, Y.;

Graphical Abstract

Modulating Water Binding in Branched Poly(terphenylene 3-piperidinium) Anion Exchange Membranes for High-performance Water Electrolysis

Zhen-Jiang Yan, Bo Li, Chen-Xi Wang, Lan Zhang, Heng Wang, Hai-Bing Wei, and Yun-Sheng Ding

Hefei University of Technology; University of Chinese Academy of Sciences, Chinese Academy of Sciences

A branched poly(terpolyphenylene 3-piperidinium) membrane was developed, featuring a high fraction of bound water and improved ion conduction efficiency. Water electrolysis cells using this membrane achieved current densities of 10.4 A·cm^{-2} at 2.0 V with an Ir anode and 6.3 A·cm^{-2} with a noble-metal-free Ni-Fe anode, and demonstrated 1000 h durability in the noble-metal-free anode configuration.

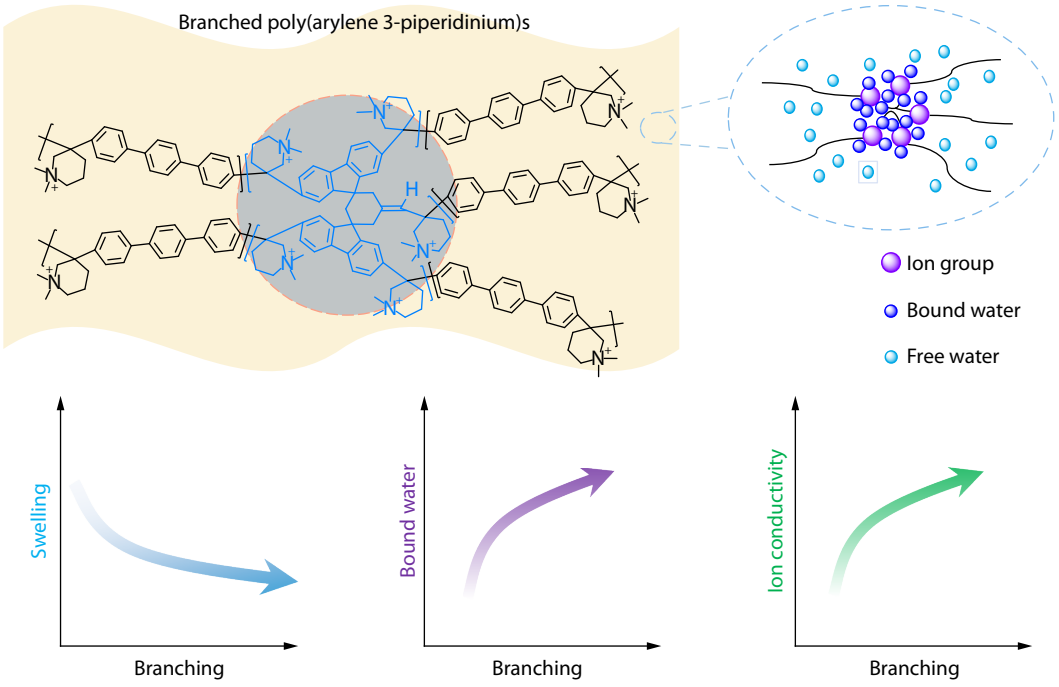

Chinese J. Polym. Sci. 2026, 44, 2502–2512 *https://doi.org/10.1007/s10118-026-3663-0*

Wei, H.; Ding, Y. Poly(spirofluorene)-based anion exchange membranes for alkaline electrochemical energy devices. *Macromolecules* **2024**, *57*, 5461–5471.

18 Ren, Z. W.; Zhao, Y.; Han, Y. K.; Wei, T.; Sun, J. Q.; Jiao, Z. L.; Liu, X. Y.; Zhang, H. T.; Shao, Z. G. Improving alkali stability of anion exchange membrane by a super water-retention strategy. *Adv. Funct. Mater.* **2025**, *35*, 2423460.

19 Gottesfeld, S.; Dekel, D. R.; Page, M.; Bae, C.; Yan, Y.; Zelenay, P.; Kim, Y. S. Anion exchange membrane fuel cells: Current status and remaining challenges. *J. Power Sources* **2018**, *375*, 170–184.

20 Li, Z. L.; Lu, S. W.; Gao, L.; Ruan, X. H.; Jiang, X. B.; Yan, X. M.; He, G. H. Cyclophane-architected piperidinium polymers with intrinsic microporosity boost ion transport in high-performance anion exchange membrane fuel cells. *Adv. Funct. Mater.* **2025**, *35*, 2511710.

21 Liu, Z. Q.; Lin, K. J.; Yin, W. M.; Liang, L. B.; Zhu, Y. Q. High-performance side-chain-type anion exchange membranes with triptycene-based hydrophobic segments. *J. Membr. Sci.* **2024**, *708*, 123034.

22 Gu, Y.; Piao, B. X.; Ma, T. Y.; Xu, S. C.; He, R. H. Stereo-branching of poly(aryl piperidinium) by dianthracene for preparing membrane electrolytes with enhanced properties and using in alkaline water electrolytic cells. *J. Membr. Sci.* **2026**, *740*, 124989.

23 Hu, C.; Kang, N. Y.; Kang, H. W.; Lee, J. Y.; Zhang, X.; Lee, Y. J.; Jung, S. W.; Park, J. H.; Kim, M.-G.; Yoo, S. J.; Lee, S. Y.; Park, C. H.; Lee, Y. M. Triptycene branched poly(aryl-co-aryl piperidinium) electrolytes for alkaline anion exchange membrane fuel cells and water electrolyzers. *Angew. Chem. Int. Ed.* **2024**, *63*, e202316697.

24 Tang, T.; Lee, H.; Wang, Z.; Li, Z.; Wang, L.; Chen, D.; Zheng, W.; Liu, Q.; He, L.; Ding, G.; Tian, Z.; Sun, L. Bioinspired anion exchange membranes with dual steric cross-linking centers for industrial-scale water electrolysis. *Energy Environ. Sci.* **2024**, *17*, 7816–7828.

25 Wu, X.; Chen, N.; Klok, H.-A.; Lee, Y. M.; Hu, X. Branched poly(aryl piperidinium) membranes for anion-exchange membrane fuel cells. *Angew. Chem. Int. Ed.* **2022**, *61*, e202114892.

26 Zhang, H.; Xu, W.; Song, W.; Peng, K.; Sun, L.; Yang, C.; Zhang, X.; Zhang, H.; Ye, B.; Liang, X.; Yang, Z.; Wu, L.; Ge, X.; Xu, T. High-performance spiro-branched polymeric membranes for sustainability applications. *Nat. Sustain.* **2024**, *7*, 910–919.

27 Talipov, M. R.; Abdelwahed, S. H.; Thakur, K.; Reid, S. A.; Rathore, R. From wires to cables: attempted synthesis of 1,3,5-trifluorenylcyclohexane as a platform for molecular cables. *J. Org. Chem.* **2016**, *81*, 1627–1634.

28 Wang, A. Q.; Breakwell, C.; Foglia, F.; Tan, R.; Lovell, L.; Wei, X. C.; Wong, T.; Meng, N. Q.; Li, H. D.; Seel, A.; Sarter, M.; Smith, K.; Alvarez-Fernandez, A.; Furedi, M.; Guldin, S.; Britton, M. M.; McKeown, N. B.; Jelfs, K. E.; Song, Q. Selective ion transport through hydrated micropores in polymer membranes. *Nature* **2024**, *635*, 353–358.

29 Ryoo, G. W.; Shin, S. H.; Song, I. W.; Lim, J.; Shin, H.; Kwon, K. C.; Park, S. H.; Lee, J. Y.; Kwon, M. S. Poly(aryl piperidinium)-based AEMs utilizing spirobifluorene as a branching agent. *Adv. Funct. Mater.* **2024**, *34*, 2408545.

30 Maurya, S.; Noh, S.; Matanovic, I.; Park, E. J.; Narvaez Villarrubia, C.; Martinez, U.; Han, J.; Bae, C.; Kim, Y. S. Rational design of polyaromatic ionomers for alkaline membrane fuel cells with >1 W cm^{-2} power density. *Energy Environ. Sci.* **2018**, *11*, 3283–3291.

31 Yang, K.; Li, X. F.; Guo, J.; Zheng, J. F.; Li, S. H.; Zhang, S. B.; Cao, X. Z.; Sherazi, T. A.; Liu, X. Q. Preparation and properties of anion exchange membranes with exceptional alkaline stable polymer backbone and cation groups. *J. Membr. Sci.* **2020**, *596*, 117720.

32 Liu, Q.; Gao, H. M.; Liu, B. H.; Han, J. S.; Pang, Y.; Zhao, C. J. Effect of branching degree of quaternized poly(p-terphenyl p-terphenyl isatin) on the performance of anion exchange membrane water electrolyzers. *J. Membr. Sci.* **2024**, *709*, 123133.

33 Su, X.; Nan, S. B.; Wei, W.; Xu, S. C.; He, R. H. Highly conductive and robustly stable anion exchange membranes with a star-branched crosslinking structure. *J. Membr. Sci.* **2023**, *683*, 121843.

34 Zhao, J. L.; Gao, J.; Lei, Y. J.; Sun, S. Y.; Wu, J. Y.; Li, N.; Lu, J. H.; Chang, Y. F.; Yang, J. Y.; Wang, Z. Synergistic effect of localized three-dimensional polymer backbone and self-assembling cation for the construction of novel anion exchange membrane. *Macromolecules* **2024**, *57*, 9823–9832.

35 Yang, J. Y.; Zhao, J. L.; Li, N.; Sun, S. Y.; Lei, Y. J.; Wu, J. Y.; Lin, X. H.; Wang, Z. Branched poly(aryl piperidinium) anion exchange membranes with microphase separation for fuel cells. *Macromolecules* **2025**, *58*, 6260–6270.

36 Jeon, S.; Kang, H. W.; Min, K.; Lee, W.; Maeng, H.; Park, C. H.; Kim, T. H. Hyperbranched-type anion exchange membranes with electrostatic interactions for high performance anion exchange membrane water electrolysis. *J. Membr. Sci.* **2025**, *726*, 124050.

37 Han, L.; Gong, S. T.; Zhang, H. Y.; Yang, M.; Javed, O.; Yan, X. M.; He, G. H.; Zhang, F. X. High performance anion exchange membrane containing large, rigid branching structural unit for fuel cell and electrodialysis applications. *J. Membr. Sci.* **2025**, *717*, 123552.

38 Yang, J. Y.; Zhao, J. L.; Li, N.; Lei, Y. J.; Wu, J. Y.; Gao, J.; Sun, S. Y.; Feng, K. R.; Wang, Y.; Wang, Z. Carbazole-based branched poly(aryl piperidinium) membranes for ultra-stable anion exchange membrane fuel cells. *Chem. Eng. J.* **2024**, *489*, 151446.

39 Han, L.; Gong, S. T.; Zhang, X. L.; Yang, M.; Yan, X. M.; He, G. H.; Zhang, F. X. Four-arm star-shaped high-performance poly(aryl piperidine) anion exchange membranes for fuel cells. *J. Mater. Chem. A* **2024**, *12*, 6341–6350.

40 Jiang, T.; Zhou, Y.; Yang, Y.; Wu, C.; Fang, H.; Yang, S.; Wei, H.; Ding, Y. Dimensionally and oxidatively stable anion exchange membranes based on bication cross-linked poly(meta-terphenylene alkylene)s. *Polymer* **2021**, *216*, 123433.

41 Zou, W. H.; Peng, K.; Ling, R.; Li, Q. X.; Liu, Y. L.; Xu, T. W.; Yang, Z. J. Robust and ultrathin pore-filling anion exchange membranes for water electrolysis. *AIChE J.* **2025**, *71*, e18769.

42 Ling, Q.; Wang, C.; Wang, T.; Yang, S.; Li, X.; Wei, H.; Ding, Y. Beyond small molecular cations: elucidating the alkaline stability of cationic moieties at the membrane scale. *ChemSusChem* **2024**, *17*, e202301656.

43 Wang, C.; Wang, T.; Chen, D.; Ling, Q.; Liu, C.; Li, X.; Wei, H.; Ding, Y. Insights into the alkaline stability of poly(arylene piperidinium)s. *Macromolecules* **2025**, *58*, 8335–8343.

44 Wang, T.; Chen, D.; Wang, C.; Wei, H.; Ding, Y. Isomeric poly(arylene piperidinium) electrolyte membranes with high alkaline durability. *Adv. Funct. Mater.* **2025**, *35*, 2422504.

45 Olsson, J. S.; Pham, T. H.; Jannasch, P. Poly(arylene piperidinium) hydroxide ion exchange membranes: synthesis, alkaline stability, and conductivity. *Adv. Funct. Mater.* **2018**, *28*, 1702758.

46 Li, D. G.; Matanovic, I.; Lee, A. S.; Park, E. J.; Fujimoto, C.; Chung, H. T.; Kim, Y. S. Phenyl oxidation impacts the durability of alkaline membrane water electrolyzer. *ACS Appl. Mater. Interfaces* **2019**, *11*, 9696–9701.

47 Nemeth, T.; Nauser, T.; Gubler, L. On the radical-induced degradation of quaternary ammonium cations for anion-exchange membrane fuel cells and electrolyzers. *Chemsuschem* **2022**, *15*, e202201571.

48 Li, Z.; Lin, G.; Wang, L.; Lee, H.; Du, J.; Tang, T.; Ding, G.; Ren, R.; Li, W.; Cao, X.; Ding, S.; Ye, W.; Yang, W.; Sun, L. Seed-assisted formation of NiFe anode catalysts for anion exchange membrane water electrolysis at industrial-scale current density. *Nat. Catal.* **2024**, *7*, 944–952.

49 Wu, L. Z.; Wang, Q.; Yuan, S.; Mei, X. H.; Wang, Q.; Zou, X. H.; Zhang, K.; Huo, X. Y.; Shi, X. Y.; Pan, Z. F.; Yan, X.; An, L. Unrevealing the interaction between electrode degradation and bubble behaviors in an anion exchange membrane water electrolyzer. *Adv. Sci.* **2025**, *12*, 2412.